2004

The Parsec-Scale Structure and Jet Motions of the TeV Blazars 1ES 1959+650, PKS 2155-304, and 1ES 2344+514

B. Glenn Piner
gpiner@whittier.edu

Philip G. Edwards

Recommended Citation

Piner, B. G., & Edwards, P. G. (2003). The Parsec-Scale Structure and Jet Motions of the TeV Blazars 1ES 1959+650, PKS 2155-304, and 1ES 2344+514. Astrophysical Journal, 600, 115-126. https://doi.org/10.1086/379769

The Astrophysical Journal, 600:115–126, 2004 January 1

THE PARSEC-SCALE STRUCTURE AND JET MOTIONS OF THE TeV BLAZARS 1ES 1959+650, PKS 2155−304, AND 1ES 2344+514

B. Glenn Piner[1,2] and Philip G. Edwards[3]
Received 2003 August 5; accepted 2003 September 11

ABSTRACT

As part of our study of the VLBI properties of TeV blazar jets, we present here a series of high-resolution 15 GHz Very Long Baseline Array (VLBA) images of the parsec-scale jets of the TeV blazars 1ES 1959+650, PKS 2155−304, and 1ES 2344+514, with linear resolutions of ∼0.5 pc. Each of these sources was observed with the VLBA at three or four epochs during 1999 and 2000. There is a notable lack of any strong moving components on the VLBI images (in contrast to the rapid superluminal motions seen in EGRET blazars), and the structure of the VLBI jet can be modeled either as a series of stationary Gaussian components or as a smooth power law for two of the sources (PKS 2155−304 and 1ES 2344+514). The low apparent speeds, together with beaming indicators such as the brightness temperature of the VLBI core, imply only modest Doppler boosting of the VLBI radio emission and only modest bulk Lorentz factors (δ and $\Gamma \approx$ a few), in contrast to the more extreme values of these parameters invoked to explain the high-energy emission. The fact that no moving shocks or plasmoids are seen on the parsec scale suggests that the shocks or plasmoids that are assumed to be responsible for the high-energy flares must dissipate before they separate from the core on the VLBI images. This requires the loss of a substantial amount of bulk kinetic energy on parsec scales and implies a higher efficiency than is typically assumed for internal shock scenarios.

Subject headings: BL Lacertae objects: individual (1ES 1959+650, 1ES 2344+514, PKS 2155−304) — galaxies: active — galaxies: jets — radio continuum: galaxies

1. INTRODUCTION

The blazar phenomenon is well established to be the result of relativistic electrons (and possibly positrons) radiating in a jet that is undergoing bulk relativistic motion at a small angle to the observer's line of sight. The characteristic blazar spectral energy distribution is two-peaked, with the low-frequency peak due to synchrotron radiation and the high-frequency peak due to inverse Compton scattering, either of the jets own synchrotron photons (synchrotron self-Compton or SSC emission) or of external photons (the so-called external-radiation Compton, or ERC, emission). In VLBI images, most blazars display rapid superluminal apparent motions (Jorstad et al. 2001a). A particular subclass of blazar whose synchrotron spectra in a νF_ν plot peak at X-ray frequencies (the high-frequency peaked BL Lac objects, or HBLs) has inverse Compton spectra that peak at TeV γ-ray frequencies, and a few of these objects have been detected by ground-based TeV γ-ray telescopes (Horan et al. 2002). This set of objects is referred to as the TeV blazars. The TeV blazars are restricted to relatively nearby HBLs, because of the absorption of TeV γ-rays by pair-production on the extragalactic background light.

The TeV blazars display a number of interesting characteristics: They show dramatic variability in their high-energy emission (e.g., Gaidos et al. 1996), and the size scales implied by such rapid variability require large relativistic Doppler factors in the γ-ray producing region to avoid γ-ray absorption [the Doppler factor $\delta = 1/\Gamma(1-\beta\cos\theta)$, where Γ is the bulk Lorentz factor, $\beta = v/c$, and θ is the angle to the line of sight]. Some specific emission models require extreme Doppler factors and bulk Lorentz factors (∼40–50); these values can be somewhat reduced in some models but remain high (∼15; Georganopoulos & Kazanas 2003). The TeV blazar phenomenon thus requires both high particle and bulk Lorentz factors. The high-particle Lorentz factors that are required to produce the high-frequency emission are commonly assumed to be produced at shocks in the jet, where some of the bulk kinetic energy of the flow is converted to internal kinetic energy. These shocks may be produced either by internal interactions in the jet (e.g., Spada et al. 2001) or by interaction of the jet with the external environment (e.g., Dermer & Chiang 1998).

This paper is part of our ongoing program to study the parsec-scale jets of a TeV γ-ray–selected sample of blazars using the National Radio Astronomy Observatory's Very Long Baseline Array (VLBA).[4] VLBI observations of these TeV sources provide the highest resolution images of these jets currently achievable. These images provide independent constraints on parameters that are crucial for modeling the jet. Observations of changes in jet structure on parsec scales (superluminal motion) can constrain both the Lorentz factor of the jet and the angle of the jet to the line of sight [the apparent jet speed $\beta_{\rm app} = \beta\sin\theta/(1-\beta\cos\theta)$], and also the jet opening angle. In addition, there is the possibility of directly imaging the shock, or "component," responsible for the γ-ray flare emission, as has apparently been done for some EGRET blazars (Jorstad et al. 2001b). The VLBI observations probe

[1] Department of Physics and Astronomy, Whittier College, 13406 East Philadelphia Street, Whittier, CA 90608; gpiner@whittier.edu.
[2] NASA Summer Faculty Fellowship, Jet Propulsion Laboratory, California Institute of Technology, 4800 Oak Grove Drive, Pasadena, CA 91109.
[3] Institute of Space and Astronautical Science, Yoshinodai, Sagamihara, Kanagawa 229-8510, Japan; pge@vsop.isas.ac.jp.

[4] The National Radio Astronomy Observatory is a facility of the National Science Foundation operated under cooperative agreement by Associated Universities, Inc.

the inner-jet properties through direct imaging, and these properties can then be compared with those deduced from light curves and multiwavelength spectra.

There are currently five extragalactic sources whose detection in TeV γ-rays has been confirmed by multiple detections; all of these are HBLs. They are Mrk 421, Mrk 501, 1ES 1959+650, and H1426+428 (Horan et al. 2003 and references therein), and PKS 2155−304, which has recently been confirmed (Djannati-Ataï et al. 2003b). In addition, there have been unconfirmed detections of five other sources: the HBL 1ES 2344+514, the low-frequency peaked BL Lac objects BL Lac and 3C 66A (Horan et al. 2002 and references therein), the radio galaxy M87 (Aharonian et al. 2003a), and the starburst galaxy NGC 253 (Itoh et al. 2002). The confirmed detections of five HBLs make the TeV emission of this class of object well established, and we therefore restrict our sample to the six TeV-detected HBLs (the five confirmed sources mentioned above plus 1ES 2344+514), until such time as the TeV emission from one of the other classes of candidate objects is confirmed.

Our earlier observations of Mrk 421 were presented by Piner et al. (1999); more recent VLBA observations following the prolonged flaring state of Mrk 421 in early 2001 will be presented by B. G. Piner & P. G. Edwards (2004, in preparation). Observations of Mrk 501 were reported by Edwards & Piner (2002; see also Giroletti et al. 2003). This paper describes a series of VLBA observations of 1ES 1959+650, PKS 2155− 304, and 1ES 2344+514 obtained during 1999 and 2000. Initial results on these three sources were briefly presented by Piner et al. (2002), here we provide more detailed information and a fuller description and consideration of the entire data set. Because H1426+428 was not detected as a TeV source until relatively recently, it was not added to our observing campaign until 2001. Observations of H1426+428, plus additional monitoring of 1ES 1959+650 and PKS 2155−304, are underway and will be presented in a future paper. The VLBA flux densities of the three sources studied in this paper are substantially less ($\sim$100 mJy) than those of the two more well-studied TeV blazars Mrk 421 and Mrk 501 ($\sim$500 mJy).

In this paper we use the cosmological parameters measured by the *Wilkinson Microwave Anisotropy Probe* (*WMAP*) of $H_0 = 71$ km s^{-1} Mpc^{-1}, $\Omega_m = 0.27$, and $\Omega_\Lambda = 0.73$ (Bennett et al. 2003). We use the equation given in footnote 14 of Perlmutter et al. (1997) to compute the luminosity distance for nonzero Ω_Λ. When results from other papers are quoted, these results have been converted to the set of cosmological parameters given above. In § 2 we give a more detailed introduction to the three sources in this paper, in §§ 3 and 4 we discuss the VLBI observations and the results obtained from imaging and model fitting, and in § 5 we discuss the astrophysical implications of these results.

2. THE INDIVIDUAL SOURCES

2.1. *1ES 1959+650*

1ES 1959+650 ($z = 0.047$) became the third source to have its TeV emission confirmed, after Mrk 421 and Mrk 501. It was initially detected at a low significance in 1998 by the Utah Seven Telescope Array (Nishiyama et al. 2000), and it has subsequently been detected by the Whipple (Holder et al. 2003a), HEGRA (Aharonian et al. 2003b), and CAT (Djannati-Ataï et al. 2003a) experiments. The highest levels of TeV γ-ray activity were observed between 2002 May and 2002 July, when the source showed two strong flares, the strongest peaking at a flux of 5 crab with a doubling time of 7 hr (Holder et al. 2003a). TeV γ-ray observations at other times (2000–2001 and after 2002 September) have shown the source to be in a relatively quiescent state, with an average flux of only 0.05 crab in 2000–2001 (Aharonian et al. 2003b; Holder et al. 2003b). 1ES 1959+650 is also quite variable at X-ray (Giebels et al. 2002; Holder et al. 2003b) and optical (Villata et al. 2000) wavelengths. A multiwavelength spectrum is shown by Beckmann et al. (2002). A 5 GHz VLBA image is given by Bondi et al. (2001), and 5 GHz VLBA and 1.4 GHz VLA images are presented by Rector, Gabuzda, & Stocke (2003).

2.2. *PKS 2155−304*

As an archetypal X-ray–selected BL Lac object, PKS 2155−304 ($z = 0.117$) has been extensively observed by X-ray and UV satellites and ground-based optical monitoring, and it exhibits complex phenomenology in its rapid, strong, broadband variability. Recent results include descriptions of *BeppoSAX* data by Zhang et al. (2002), *XMM-Newton* data by Edelson et al. (2001), optical polarimetric monitoring by Tommasi et al. (2001), and a long-look *ASCA* observation by Tanihata et al. (2001). This source was detected in TeV γ-rays in late 1996 and late 1997 by the University of Durham Mark 6 Telescope, with a combined significance of 6.8 σ (Chadwick et al. 1999). The peak TeV flux was measured in 1997 November, when PKS 2155−304 was in an X-ray–high state (Chadwick et al. 1999; Chiappetti et al. 1999). A confirming detection of this source in TeV γ-rays has been made recently by the H.E.S.S. collaboration (Djannati-Ataï et al. 2003b). Specific emission models used to explain the spectra and variability of this source have used Doppler factors ranging from $\delta \sim 20$–30 (Chiappetti et al. 1999; Kataoka et al. 2000); however, the observations on which these results are based have been disputed by Edelson et al. (2001). Radio observations of PKS 2155−304 are sparse compared with the optical and high-energy observations, but a sequence of VLA images is presented by Laurent-Muehleisen et al. (1993).

2.3. *1ES 2344+514*

1ES 2344+514 ($z = 0.044$) was detected in TeV γ-rays by the Whipple Telescope (Catanese et al. 1998) during an active period from 1995 October to 1996 January, when it displayed one flare with a flux of 0.6 crab (a 6 σ detection), and an average flux level of 0.1 crab (excluding the flare, a 4 σ detection). Although subsequent TeV observations of this source have yielded only upper limits (e.g., Aharonian et al. 2002), it is the most secure of the unconfirmed detections, in part because 1ES 2344+514 is expected to be one of the brightest extragalactic TeV sources (Ghisellini 2003). Detection of exceptional X-ray spectral variability is reported by Giommi, Padovani, & Perlman (2000) from *BeppoSAX* observations between 1996 and 1998. They observe shifts by a factor of 30 or more in the peak frequency of the synchrotron emission, which ranged to at or above 10 keV. Rapid variability on timescales of 5000 s was also detected when the source was brightest. Detection of more moderate variability at optical wavelengths is discussed by Xie et al. (2002). VLBI images at 1.6 and 5 GHz are presented by Bondi et al. (2001), and 5 GHz VLBA and 1.4 GHz VLA images are shown by Rector et al. (2003).

TABLE 1

OBSERVATION LOG AND PARAMETERS OF THE IMAGES

				Natural Weighting			Uniform Weighting		
Source	Epoch	Time on Source (hr)	VLBA Antennas[a]	Beam[b]	Peak Flux Density (mJy beam^{-1})	Lowest Contour[c] (mJy beam^{-1})	Beam[b]	Peak Flux Density (mJy beam^{-1})	Lowest Contour[b] (mJy beam^{-1})
1ES 1959+650	2000 Mar 6	6	No KP, OV	0.95, 0.47, 7.6	96	0.25	0.74, 0.33, 9.5	85	0.45
	2000 Jun 9	6	All	0.95, 0.51, 10.7	96	0.23	0.70, 0.36, 15.4	82	0.44
	2000 Jul 8	6	No PT	0.91, 0.49, 9.4	98	0.28	0.68, 0.35, 15.6	85	0.50
PKS 2155−304.....	2000 Mar 3	6	All	1.38, 0.49, −1.1	210	0.34	1.01, 0.35, −2.0	194	0.62
	2000 Jun 2	6	No NL	1.49, 0.49, −3.4	137	0.33	0.99, 0.34, −0.5	124	0.95
	2000 Jun 29	6	No FD	1.41, 0.48, −5.5	155	0.38	1.00, 0.35, −1.8	143	0.82
1ES 2344+514	1999 Oct 1	8	All	0.91, 0.56, −11.6	96	0.17	0.62, 0.37, −4.8	91	0.43
	1999 Nov 9	8	All	0.91, 0.55, −10.7	93	0.18	0.63, 0.37, −4.7	89	0.40
	2000 Jan 7	8	All	0.92, 0.56, −11.3	78	0.17	0.63, 0.37, −4.0	73	0.39
	2000 Mar 23	8	No PT	0.84, 0.51, −7.9	90	0.20	0.62, 0.36, −4.0	85	0.37

[a] VLBA telescope locations are as follows: FD = Fort Davis, Texas, KP = Kitt Peak Arizona, NL = North Liberty, Iowa, OV = Owens Valley, California, and PT = Pietown, New Mexico.

[b] Numbers given for the beam are FWHMs of the major and minor axes in milliarcseconds and the position angle of the major axis in degrees. Position angle is measured from the north through the east.

[c] The lowest contour is set to be 3 times the rms noise in the image. Successive contours are each a factor of 2 higher.

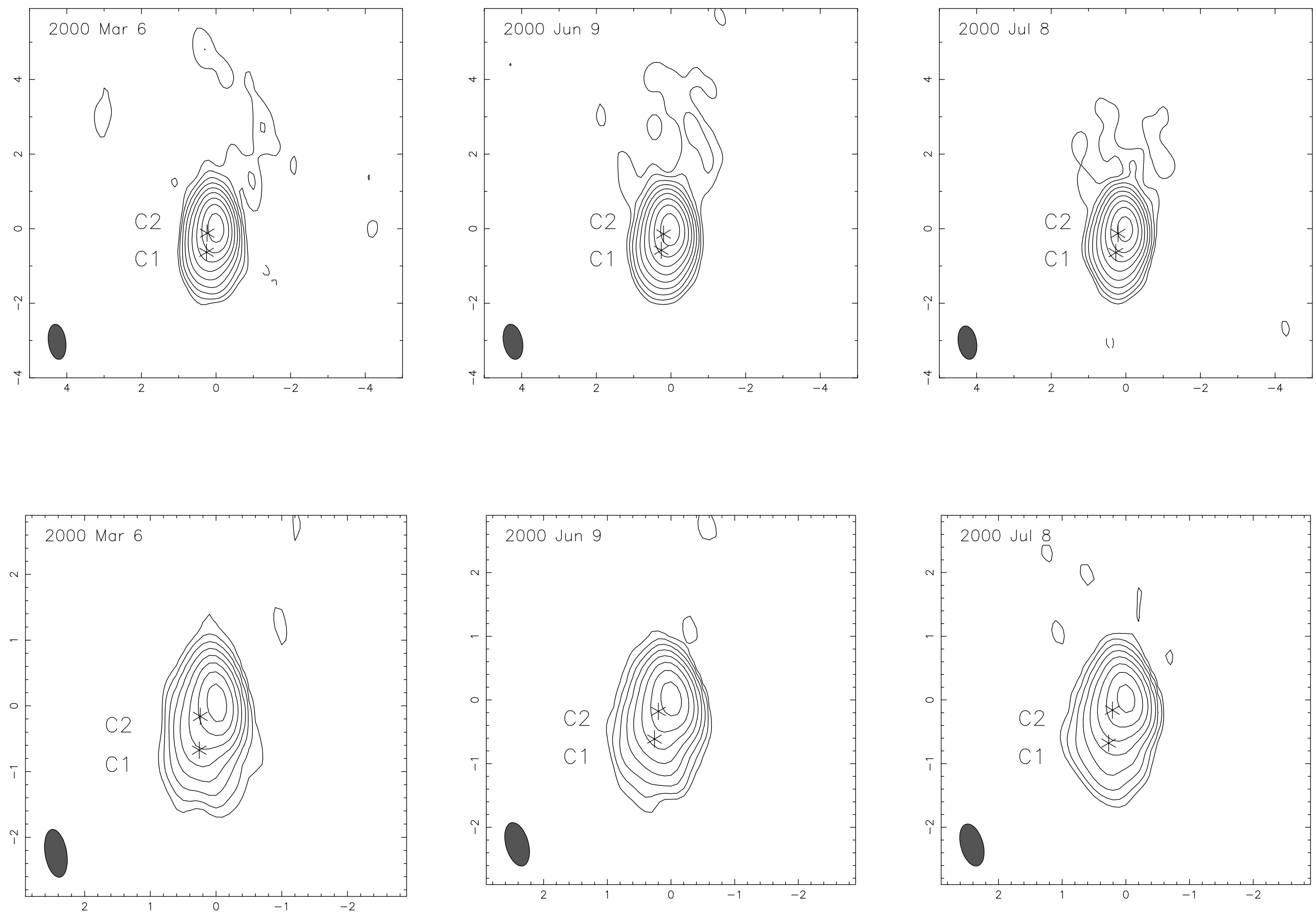

FIG. 1.—VLBA images of 1ES 1959+650 at 15 GHz. The epoch of observation is shown in the upper left corner of each image. The top row shows the images obtained with natural weighting (uvweight = 0,–2 in DIFMAP), and the bottom row shows the images obtained with uniform weighting (uvweight = 2, 0 in DIFMAP). The axes are labeled in milliarcseconds. Numerical parameters of the images are given in Table 1. The centers of the circular Gaussians (excluding the Gaussian representing the core) that were fitted to the visibilities are marked with asterisks, and the identifications of the Gaussians are indicated. Numerical parameters of these Gaussians are given in Table 2.

3. OBSERVATIONS

3.1. *Details of Observations*

We observed 1ES 2344+514 with the VLBA at 15 GHz at four epochs between 1999 October and 2000 March with 8 hr of observation time per epoch (a total of 32 hr), under observation code BP057. We observed 1ES 1959+650 and PKS 2155−304 at 15 GHz at three epochs each between 2000 March and 2000 July with 6 hr of observation time per source per epoch (a total of 36 hr), under observation code BP062. All of the observations used standard VLBA continuum setups (eight intermediate frequencies, 64 MHz total bandwidth, 1 bit sampling for BP057; four intermediate frequencies, 32 MHz total bandwidth, 2 bit sampling for BP062), and all recorded left circular polarization. An observation log is given in Table 1. An observing frequency of 15 GHz was chosen because it provided the best combination of the high resolution needed to monitor possible moving jet components with the sensitivity required to image jets in these relatively faint ∼100 mJy sources with adequate dynamic range. Calibration and fringe-fitting were done with the AIPS software package. Images from these data sets were produced using standard CLEAN and self-calibration procedures from the DIFMAP software package (Shepherd, Pearson, & Taylor 1994). The size of the VLBA beam at 15 GHz is approximately 0.5 mas; this corresponds to linear resolutions of about 0.5 pc for 1ES 1959+650 and 1ES 2344+514, and about 1 pc for PKS 2155−304.

3.2. *Images*

The VLBA images of 1ES 1959+650, PKS 2155−304, and 1ES 2344+514 are shown in Figures 1–3, respectively. In each of these figures, the top row contains the higher sensitivity but lower resolution naturally weighted images (uvweight = 0, −2 in DIFMAP), while the bottom row contains the lower sensitivity but higher resolution uniformly weighted images (uvweight = 2, 0 in DIFMAP). Parameters of these images are given in Table 1. The rms noise in the images is approximately equal to the thermal noise limit for 1ES 2344+514 and 1ES 1959+650, for PKS 2155−304 it is about 30% higher. The dynamic range (peak/rms) achieved exceeds 1000 : 1 at all epochs for the naturally weighted images.

1ES 1959+650 has an intriguing morphology. The uniformly weighted images in Figure 1 clearly show a short jet extending 1 mas to the southeast of the core (presumed to be the northernmost of the three components we see, because it is

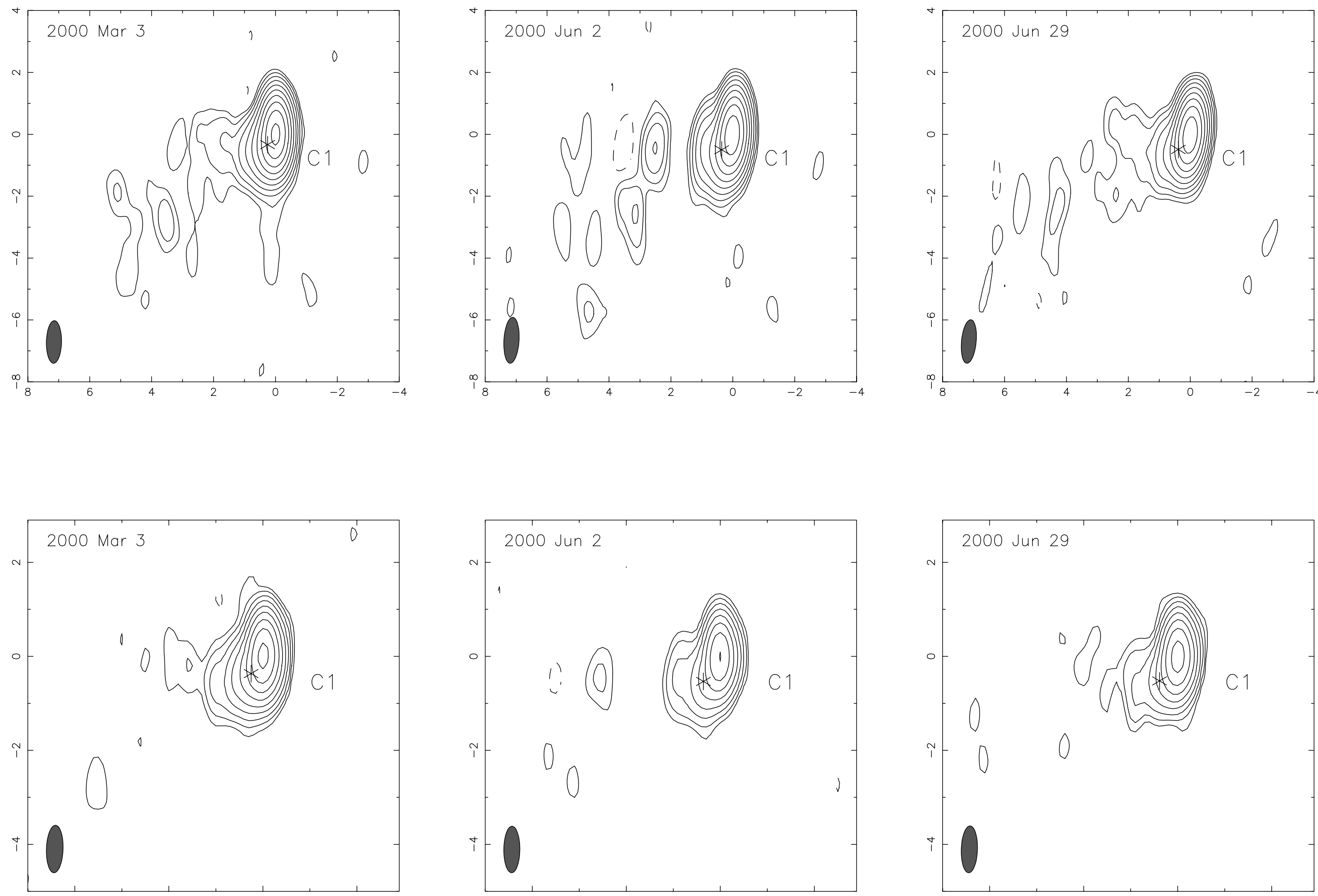

FIG. 2.—VLBA images of PKS 2155−304 at 15 GHz. The epoch of observation is shown in the upper left corner of each image. The top row shows the images obtained with natural weighting (uvweight = 0, −2 in DIFMAP), and the bottom row shows the images obtained with uniform weighting (uvweight = 2, 0 in DIFMAP). The axes are labeled in milliarcseconds. Numerical parameters of the images are given in Table 1. The centers of the circular Gaussians (excluding the Gaussian representing the core) that were fitted to the visibilities are marked with asterisks, and the identifications of the Gaussians are indicated. Numerical parameters of these Gaussians are given in Table 2.

both the brightest and the most compact), along a position angle of $\approx 160°$. The naturally weighted images also show this southeastern jet but in addition show broad, diffuse emission to the north of the core. The lower resolution 5 GHz VLBA image of 1ES 1959+650 by Rector et al. (2003; see also the similar image by Bondi et al. 2001) shows a diffuse jet with a broad ($\sim 55°$) opening angle extending 20 mas north of the core along a position angle of $\approx -5°$. There is no indication of a southern jet in those image, but the southern jet seen in this paper would not be resolved by those observations. The VLA image of Rector et al. (2003) shows faint extended flux to the north (P.A. $\approx -5°$) and south (P.A. $\approx 175°$) of the core. Because no southern jet is visible in the lower resolution 5 GHz image, we do not think the VLBA images are showing a jet and counterjet but instead speculate that the jet from this source may be very closely aligned with the line of sight, such that a slight bend carries the jet across the line of sight and causes it to appear first to the south of the core in the 15 GHz VLBA images and then to the north of the core in the 5 GHz VLBA image.

PKS 2155−304 has a jet that starts to the southeast of the core at a position angle of $\approx 150°$, before bending toward the east at about 1 mas from the core. At that point the jet becomes broader and more diffuse, before finally bending again to the southeast at about 3 mas from the core. As far as we know, these are the first published VLBI images of this source. The highest resolution VLA image of PKS 2155−304 presented by Laurent-Muehleisen et al. (1993) shows a knot nearly 180° misaligned from the VLBA jet in Figure 2; the lower resolution VLA images by these same authors also show an extended halo of emission around the core. Both 1ES 1959+650 and PKS 2155−304 show extreme jet misalignments, either in their parsec-scale structure or between the parsec and kiloparsec scales.

1ES 2344+514 shows a typical core-jet morphology, with a nearly straight jet along a position angle of $\approx 145°$, detectable out to 4 mas from the core in our images. The 5 GHz VLBA image of Rector et al. (2003; see also the similar image by Bondi et al. 2001) shows this jet extending to 50 mas from the core, but becoming more diffuse and broadening into a cone with a $\sim 35°$ opening angle. The VLA image of Rector et al. (2003) detects emission extending to the east (P.A. $\approx 105°$) in a 50° cone. The misalignment angle for this source is about 40°.

3.3. *Model Fits*

In order to quantify any possible motions in these jets, circular Gaussian model components were fit to the visibility

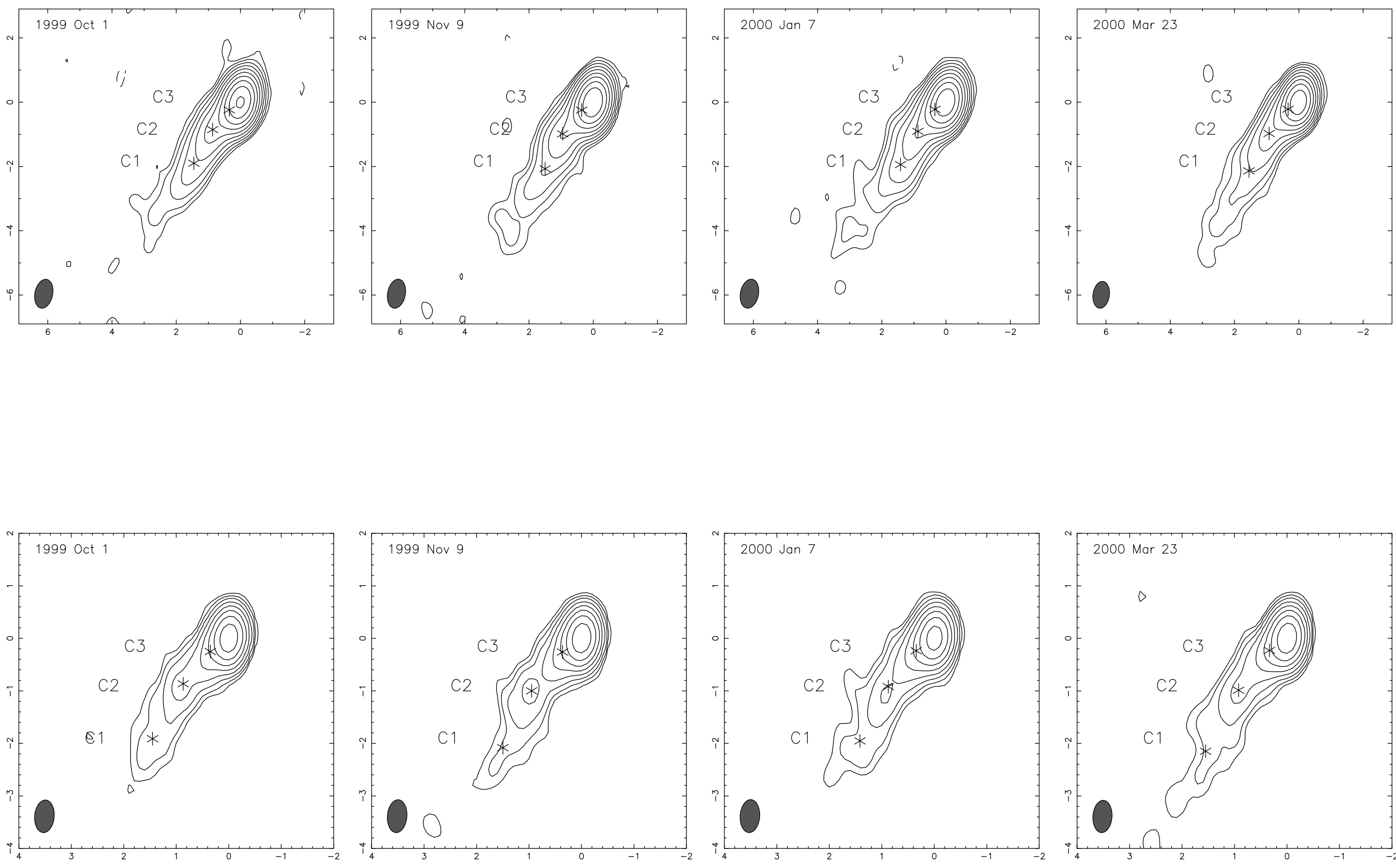

Fig. 3.—VLBA images of 1ES 2344+514 at 15 GHz. The epoch of observation is shown in the upper left corner of each image. The top row shows the images obtained with natural weighting (uvweight = 0, −2 in DIFMAP), and the bottom row shows the images obtained with uniform weighting (uvweight = 2, 0 in DIFMAP). The axes are labeled in milliarcseconds. Numerical parameters of the images are given in Table 1. The centers of the circular Gaussians (excluding the Gaussian representing the core) that were fitted to the visibilities are marked with asterisks, and the identifications of the Gaussians are indicated. Numerical parameters of these Gaussians are given in Table 2.

data using the *modelfit* task in DIFMAP. The parameters of these model fits are given in Table 2. The reduced χ^2 for all model fits was under 1.0. 1ES 1959+650 was well fitted by two circular Gaussians (C1 and C2) in addition to the core component. These components are located in the southeastern jet visible in the uniformly weighted images of Figure 1. C1 is a $\sim$20 mJy component located about 0.8 mas from the core, and C2 is a $\sim$30 mJy component located about 0.4 mas from the core. The visibilities for PKS 2155−304 are well fitted by only a single circular Gaussian in addition to the core, with a flux density $\sim$40 mJy and a core separation of $\approx$0.6 mas. The jet in 1ES 2344+514 is fitted by three Gaussians (C1, C2, and C3). The flux densities of C1, C2, and C3 are $\sim$5, 10, and 15 mJy, and the core separations are $\approx$2.5, 1.3, and 0.5 mas, respectively. The centers of the model-fit Gaussian components are marked by asterisks in Figures 1–3.

We estimate that these full-track observations allow us to measure the positions of the component centers to within 10% of a uniform beam width, and this is the error assumed for subsequent analysis (calculated by taking 10% of the projection of the elliptical beam FWHM onto a line joining the center of the core to the center of the component). Error bars larger than this produce a scatter about the fits to linear component motion that are so small as to be statistically unlikely, confirming that our estimated error is reasonable. Note that the low rms noise achieved by these long integrations allows us to detect even the faintest component (the 5 mJy C1 in 1ES 2344+514) with a signal-to-noise ratio exceeding 50 : 1.

Because the jets of these three sources appear relatively smooth, we have also investigated whether the jets can be represented by a smoothly varying function such as a power law, rather than a series of discrete Gaussians. We used the method of Xu et al. (2000), who fit the jets of FR I radio galaxies with power laws by first subtracting a Gaussian core component and then producing a one-dimensional curve of summed flux density across the jet versus distance along the jet. Xu et al. (2000) adequately fit such curves (which we hereafter refer to as jet "profiles"), which they constructed for their sample of radio galaxies with power laws with an index of about −2.

In Figure 4 we first show the jet profiles, including the core component, obtained from the CLEAN images (*solid curves*), along with the corresponding profiles obtained from the Gaussian components that were fitted to the visibilities (*dotted curves*). The vertical lines indicate the centers of the model-fit Gaussians. In Figure 5 we show the jet profiles with the core component subtracted (*solid curves*) along with the power law that is the best fit to this jet profile (*dotted curves*). We show these curves for the three sources considered in this paper and for a 15 GHz observation of the TeV blazar Mrk 501 from data presented by Edwards & Piner (2002). Both smooth power laws (with fitted indices that fall between −1 and −2) and a series of discrete Gaussians that sum to produce an

TABLE 2

Circular Gaussian Models

Source	Epoch	Component	S^a (mJy)	r^b (mas)	P.A.[b] (deg)	a^c (mas)
1ES 1959+650	2000 Mar 6	Core	91	. . .	. . .	0.14
		C2	25	0.37	134.0	0.29
		C1	18	0.82	159.9	0.56
	2000 Jun 9	Core	83	. . .		0.15
		C2	31	0.35	140.5	0.27
		C1	22	0.76	158.1	0.52
	2000 Jul 8	Core	85	. . .	. . .	0.14
		C2	36	0.35	137.1	0.27
		C1	19	0.83	159.0	0.59
PKS 2155−304.....	2000 Mar 3	Core	205	. . .	. . .	0.18
		C1	52	0.53	150.2	0.75
	2000 Jun 2	Core	138	. . .	. . .	0.18
		C1	33	0.70	149.3	0.53
	2000 Jun 29	Core	165	. . .	. . .	0.21
		C1	26	0.71	146.1	0.68
1ES 2344+514	1999 Oct 1	Core	93	. . .	. . .	0.08
		C3	13	0.46	129.0	0.23
		C2	10	1.26	135.9	0.46
		C1	5	2.44	143.2	0.76
	1999 Nov 9	Core	92	. . .	. . .	0.10
		C3	13	0.47	128.6	0.24
		C2	9	1.41	137.2	0.52
		C1	4	2.60	144.6	0.94
	2000 Jan 7	Core	75	. . .	. . .	0.11
		C3	14	0.45	127.6	0.23
		C2	8	1.31	137.2	0.51
		C1	5	2.45	144.3	0.85
	2000 Mar 23	Core	87	. . .	. . .	0.09
		C3	16	0.44	127.9	0.23
		C2	10	1.39	137.7	0.62
		C1	4	2.69	144.5	0.93

[a] Flux density in millijanskys.
[b] P.A. and r are the polar coordinates of the center of the component relative to the presumed core. Position angle is measured from north through east.
[c] FWHM of the circular Gaussian component.

approximately smooth curve are adequate fits to the observed jet profiles for PKS 2155−304 and 1ES 2344+514. The jet profile of 1ES 1959+650 does show a smooth decline, but this curve is not well fitted by a power law. The jet profile of Mrk 501 has local maxima, and would not be well fitted by any monotonic function. Note that the jet profile of 1ES 2344+514 also shows small local maxima near the locations of the model-fit Gaussians.

There are then two possibilities. It is possible that these three jets are intrinsically a series of discrete components that are blended into an approximately smooth profile by the limited resolution close to the core. It is also possible that the jet has an intrinsically smooth profile that is being reproduced in the model fitting by the appropriate sum of discrete Gaussians. Given the limited range over which we can follow these low flux density jets, we can not distinguish between these two possibilities using only the data from these three sources, and both discrete Gaussians and power laws provide about equally good fits to the jet profiles, for two of the three sources (1ES 1959+650 is better fitted by Gaussians).

To resolve this issue, we return to our observations of the TeV sources Mrk 421 (Piner et al. 1999) and Mrk 501 (Edwards & Piner 2002), which are very similar to the three sources studied here except that their radio flux density is nearly an order of magnitude higher and their jets can therefore be followed further from the core and with higher dynamic range. In Mrk 421 and Mrk 501, it is evident from jet profile plots that these jets show a series of local maxima and minima, that are much better fit by Gaussian components than by a smooth power law. The profiles of Mrk 501 are shown in Figures 4 and 5, and plots for Mrk 421 show similar structure. By analogy with the two better observed TeV blazars, we retain the Gaussian model for source morphology in the remainder of this paper, making the assumption that the jets of the fainter (in the radio) TeV sources are similar to the jets of the brighter sources Mrk 421 and Mrk 501. Representation by Gaussians is also necessary to facilitate comparison of these sources with published VLBI data on other sources, such as the EGRET blazars (Jorstad et al. 2001a) or VLBA 2 cm survey sources (Kellermann et al. 2000), as well as with Mrk 421 and Mrk 501.

4. RESULTS

4.1. *VLBI Core*

We estimate that the flux densities of the VLBI cores given in Table 2 are accurate to within about 10%, taking into account the corrections made by amplitude self-calibration and estimated errors in the model fits. With 10% error bars there is no significant detection of core flux density variability,

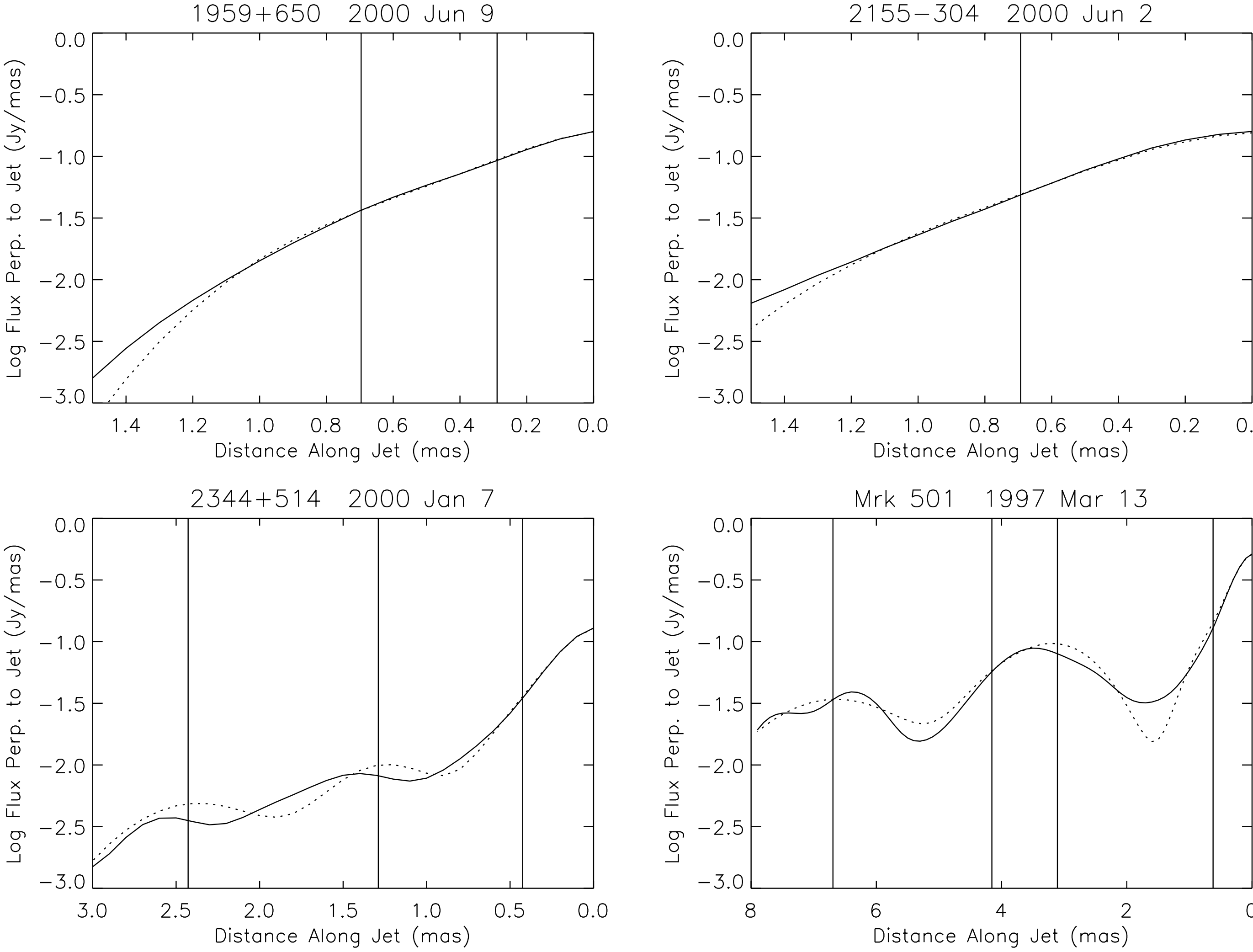

FIG. 4.—Jet profiles showing the summed flux across the jet as a function of distance along the jet for 1959+650 on 2000 June 9, 2155−304 on 2000 June 2, 2344+514 on 2000 January 7, and Mrk 501 on 1997 March 13. Data on Mrk 501 are from a 15 GHz observation from Edwards & Piner (2002). The solid curves show the summed flux from the CLEAN image, and the dotted curves show the profiles produced by the Gaussian models that were fitted to the visibility data from Table 2. The vertical lines show the positions of the centers of the Gaussians that compose the Gaussian model.

except in the case of PKS 2155−304, for which there is a marginal detection of variability, with a 0.025 χ^2 probability of constant flux density. The VLBI core flux density of this source decreases by 30% between 2000 March and 2000 June and then increases again by 20% by the end of 2000 June.

From the core flux densities and measured sizes we can calculate the brightness temperature, which can be used as an indicator of the amount of Doppler boosting, characterized by the Doppler factor δ. The maximum brightness temperature of a circular Gaussian is given by $T_B = 1.22 \times 10^{12} S (1+ z)/a^2 \nu^2$ K, where S is the flux density of the Gaussian in janskys, a is the FWHM of the Gaussian in mas, ν is the observation frequency in GHz, and z is the redshift. Observed brightness temperatures are amplified by a factor of δ over intrinsic brightness temperatures and often lie above physical limits such as the inverse Compton limit ($\sim 10^{12}$ K; Kellermann & Pauliny-Toth 1969) and equipartition limit ($\sim 10^{11}$ K; Readhead 1994). A lower limit on δ can then be invoked that reduces the observed brightness temperature below the appropriate limit (e.g., Tingay et al. 2001).

The Gaussian core components in Table 2 all have similar brightness temperatures of a few times 10^{10} K, with a mean brightness temperature of 3×10^{10} K. The core components are all partially resolved, and lower limits on the core sizes (and therefore upper limits on the brightness temperature) were obtained using the DIFWRAP program for model component error analysis (Lovell 2000). The brightness temperature upper limits are about twice the best-fit values, with a mean brightness temperature upper limit of 6×10^{10} K. The equipartition brightness temperature for these three sources is $\approx 6 \times 10^{10}$ K, using equation (4a) of Readhead (1994), and therefore no relativistic beaming needs to be invoked to bring the brightness temperature below either the inverse Compton or equipartition limit. In fact, if δ is high in the VLBI core, then the core has a large departure from equipartition and minimum energy (Readhead 1994). There is thus no indication from the VLBI core properties that the core emission is highly beamed, for any of these three sources.

4.2. *VLBI Jet*

Apparent speeds for the VLBI jet components in Table 2 were measured by making linear least-square fits to the separation of the components from the VLBI core versus time.

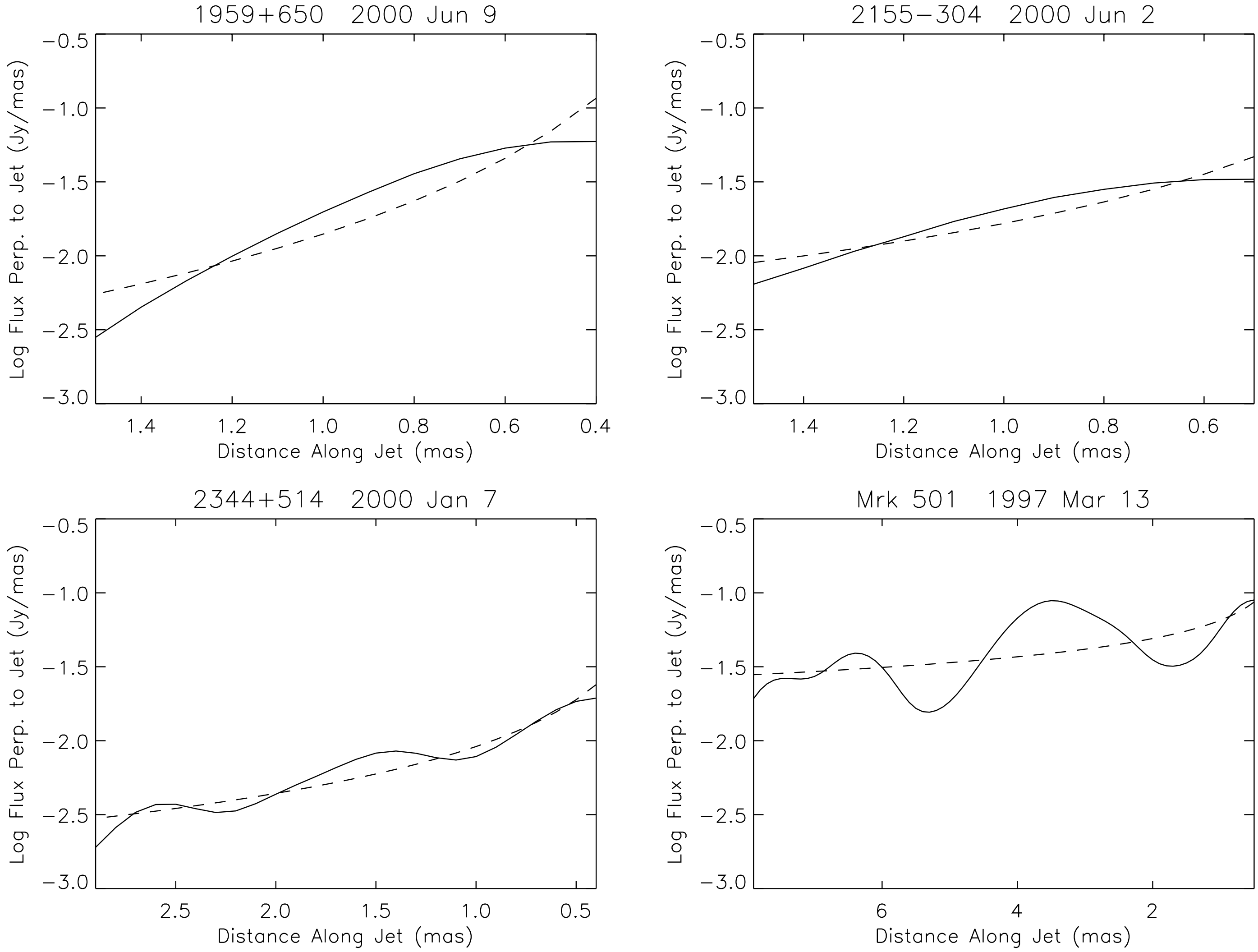

FIG. 5.—Jet profiles showing the summed flux across the jet as a function of distance along the jet for 1959+650 on 2000 June 9, 2155−304 on 2000 June 2, 2344+514 on 2000 January 7, and Mrk 501 on 1997 March 13. Data on Mrk 501 are from a 15 GHz observation from Edwards & Piner (2002). The core component has been subtracted from the image prior to the summing. The solid curves show the summed flux from the CLEAN image after the subtraction of the core, and the dotted curves show the power law that is the best fit to the solid curve.

These fits are shown in Figures 6*a*–6*c*. Fitted speeds are given in Table 3 for the three sources contained in this paper, as well as for Mrk 421 (B. G. Piner & P. G. Edwards 2004, in preparation) and Mrk 501 (Edwards & Piner 2002). The apparent component speeds are mostly subluminal, and many are consistent with no motion (stationary components). The notable exception is PKS 2155−304, but the error bar on this speed measurement is large. In fact, the measured component speeds for the three sources studied in this paper, when considered together, are statistically consistent with no motion (χ^2 probability of 0.12 for no motion of any component). Because of the slow or nonexistent component motions, there are no correlations found between VLBI component ejections and episodes of high-energy activity, as was found for the EGRET blazars by Jorstad et al. (2001b). Again, the one exception may be PKS 2155−304, where the 1 σ range on the zero-separation epoch of the jet component includes the 1997 November TeV and X-ray–high state, but this error range is large enough that this is not conclusive.

It should be noted that because of the relatively short time period spanned by these observations (4–6 months, depending on the source), any relatively slow speed will be statistically consistent with no motion. There is thus a lower limit to the speed that can be distinguished from a stationary component with this data, corresponding to $\approx 1c$ for 1ES 1959+650 and 1ES 2344+514, and $\approx 4c$ for PKS 2155−304 (this higher limit is due to the higher redshift, shorter time coverage, and more elliptical beam for this source).

5. DISCUSSION

The parsec-scale jets of the TeV blazars are different in character from the jets of the other well-studied γ-ray–selected sample, the EGRET blazars, whose VLBI properties were studied by Jorstad et al. (2001a, 2001b). A Kolmogorov-Smirnov (K-S) test comparing the apparent speeds measured in the TeV blazars (Table 3) to those measured for EGRET blazars (Jorstad et al. 2001a) shows a difference in the apparent speed distribution with 99.98% confidence, with the TeV blazars having slower apparent speeds. K-S tests also show the TeV blazar apparent speeds to be slower than those in radio-selected samples: comparison with the Caltech-Jodrell Bank Flat Spectrum (CJF) Survey (Vermeulen 1995)

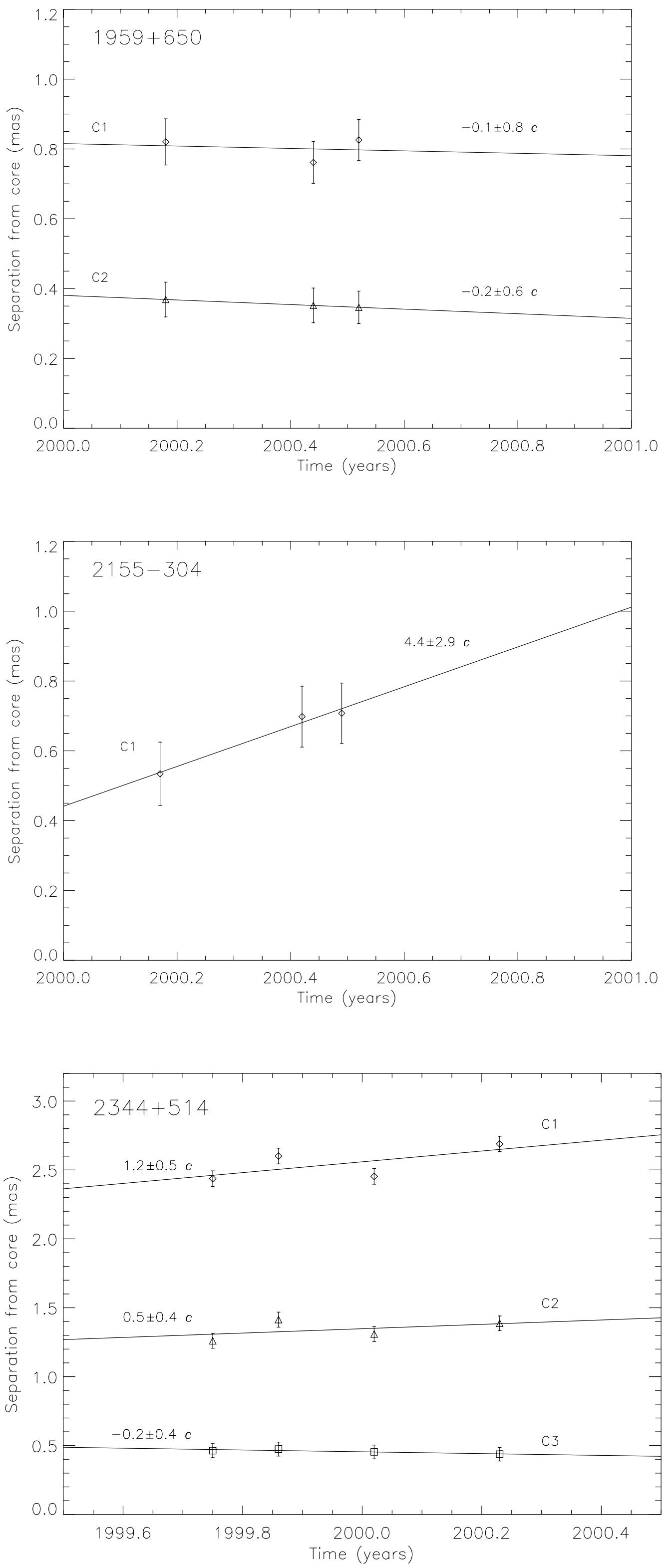

FIG. 6.—(*a*)–(*c*): Distances from the core of Gaussian component centers as a function of time. Error bars are 10% of the projection of the uniformly weighted beam along a line joining the center of the core to the center of the component. The lines are the least-squares fits to outward motion with constant speed. The fitted apparent speeds are shown next to these lines. (*a*) 1ES 1959+650; (*b*) PKS 2155−304; (*c*) 1ES 2344+514.

shows a difference with 99.91% confidence, and comparison with the 2 cm survey (Kellermann et al. 2000) shows a difference with a somewhat lower 97.90% confidence.

The presence of stationary components in the TeV blazars is not surprising, because in all of the VLBI surveys mentioned above, one-third to one-half of the VLBI components observed are found to be very slow or stationary. However, superluminally moving components are usually also present in the jets of these sources with stationary components, indicating that the jet is not intrinsically slow (Jorstad et al. 2001a). What causes the statistical difference in the speed distribution of the TeV blazars is not the presence of stationary components, but the lack of any superluminally moving components. This lack of any superluminally moving features is the same conclusion that would be reached if we had used the smooth power law fits to the jets (§ 3.3), but representation by Gaussians is required for the quantitative comparison given above. The important question to be answered about the parsec-scale jets of these sources is then, What has become of the relativistically moving shocks that are assumed to be responsible for the high-energy flaring activity and that are clearly visible in the jets of the EGRET blazars?

The first hypothesis that should be examined is that the moving components are present but appear slow because of a very small angle to the line of sight. The angle to the line of sight calculated from the highest measured speed (or speed upper limit) for each source is given in Table 3, for an assumed δ of 10 (a typical lower limit from models of the multiwavelength spectra and variability). These angles to the line of sight are typically less than a degree. Even though γ-ray–selected samples should have a distribution that lies closer to the line of sight than radio-selected samples (because of the dependence of the γ-ray flux on a higher power of δ; see the Monte Carlo simulations of Lister 1998), they should not typically be so close to the line of sight as to appear subluminal, and the Monte Carlo simulations of Lister (1998) predict a faster apparent speed distribution for γ-ray–selected samples, for both SSC and ERC γ-ray emission. While the extreme misalignments on parsec scales, or between parsec and kiloparsec scales, in three of these sources (Mrk 501, 1ES 1959+650, and PKS 2155−304) does indicate a fairly small angle to the line of sight, the typical angle is more likely to be a few degrees, rather than less than 1°. Note also that Giebels et al. (2002) state that the "quiescent" X-ray emission from these sources can be explained by jets aligned within a few degrees of the line of sight.

On the basis of other indications that δ in the parsec-scale radio jet is actually low (such as the low brightness temperatures), we consider the more likely explanation for the sluggish parsec-scale jets to be that the bulk Lorentz factor has been reduced between the TeV-emitting subparsec scale and the parsec scale. Such a change in the bulk Lorentz factor (from $\Gamma > 10$ to Γ of a few) also provides an explanation for problems encountered in BL Lac–FR I unification (Georganopoulos & Kazanas 2003). We note that the jet decollimation observed in all of these sources at a few milliarcseconds from the core is also indicative of a jet that has little momentum left and is easily influenced by the external medium. This morphology in Mrk 501 is interpreted by Giroletti et al. (2003) in terms of a decelerating two-component (fast inner spine and slower outer layer) jet model, based on flux profiles transverse to the jet. For the weaker sources presented in this paper, we do not have sufficient sensitivity or resolution transverse to the jet to attempt decomposition into separate spine

TABLE 3
Apparent Component Speeds in TeV Blazars

Source	Component	Apparent Speed[a] (multiples of c)	Reference	θ[b] (deg)
Mrk 421	C4	0.04 ± 0.06	1	
	C5	0.20 ± 0.05	1	0.2
	C6	0.18 ± 0.05	1	
	C7	0.12 ± 0.06	1	
	C8	0.06 ± 0.03	1	
Mrk 501	C1	0.05 ± 0.18	2	
	C2	0.54 ± 0.14	2	0.6
	C3	0.26 ± 0.11	2	
	C4	−0.02 ± 0.06	2	
1ES 1959+650	C1	−0.11 ± 0.79	3	0.8
	C2	−0.21 ± 0.61	3	
PKS 2155−304.....	C1	4.37 ± 2.88	3	4.2
1ES 2344+514	C1	1.15 ± 0.46	3	1.3
	C2	0.46 ± 0.43	3	
	C3	−0.19 ± 0.40	3	

[a] For $H_0 = 71$ km s^{-1} Mpc^{-1}, $R_m = 0.27$, and $\Omega_m = 0.73$.
[b] Angle to the line of sight calculated for an assumed Doppler factor of 10, using the highest measured component speed (or speed upper limit) for each source. This is *not* meant to be used as the actual Lorentz factor and angle to the line of sight (see text).
(1) B. G. Piner & P. G. Edwards 2003, in preparation. (2) Edwards & Piner 2002, with modified cosmological parameters. (3) This paper.

and layer components. The lack of any observed counterjets in our images, with a lower limit on the jet to counterjet brightness ratio $J > \sim 100$, limits the amount of deceleration that has occurred and constrains the bulk Lorentz factor to remain greater than ~ 2 on parsec scales. If the jets of TeV blazars are decelerating, the important question then becomes, What is the mechanism for jet deceleration, and why does it work more efficiently in the TeV blazars than the EGRET blazars?

Most scenarios for the production of TeV γ-ray flares (and superluminal VLBI components) are based on "shock-in-jet" models. In these models, shocks transfer bulk kinetic energy to internal energy of the plasma, which then radiates. The shock models can be broadly divided into two categories: internal shocks (e.g., Spada et al. 2001; Sikora & Madejski 2000), where the shocks are due to interactions of different portions of the jet with varying densities or bulk speeds and external shocks (e.g., Dermer & Chiang 1998), where the jet plasma interacts with density variations in the external medium. The efficiency of the model is a measure of how effectively the shocks transfer bulk kinetic energy from the jet. Current internal shock models for blazars (Spada et al. 2001; Tanihata et al. 2003) have low efficiency (e.g., Fig. 3 of Spada et al. 2001 shows deceleration from $\Gamma \approx 25$ to $\Gamma \approx 20$ on parsec scales). However, low efficiency was built into the Spada et al. (2001) model in order to reproduce bulk relativistic motion on parsec scales, by enforcing small differences in bulk Lorentz factors between colliding shells. Tanihata et al. (2003) suggest that the efficiency can be increased by making this difference larger, but that there may then be problems with reproducing the observed flare timescales. The efficiency of deceleration in the Dermer & Chiang (1998) model can be quite high; see, e.g., their Figure 2 shows deceleration of a plasmoid to mildly relativistic speeds on subparsec scales. Regardless of which shock mechanism is dominant, we suggest that the deceleration of the jet to relatively small bulk Lorentz factors at parsec scales has now been established as an observed property of TeV blazars and that this property of TeV blazar jets should now be used to constrain the shock models for these sources.

6. CONCLUSIONS

This paper is part of a series exploring the parsec-scale jet structure of TeV blazars through multiepoch VLBI observations. In Piner et al. (1999) we presented observations of Mrk 421, in Edwards & Piner (2002) we presented observations of Mrk 501, and in this paper we presented VLBA observations of the fainter (in the radio) TeV blazars 1ES 1959+650, PKS 2155−304, and 1ES 2344+514. All of these sources are quite similar in their VLBI properties, and our major conclusions from this study to date are the following:

1. All of these sources have similar VLBI morphologies. There is an initial collimated jet, extending to a few milliarcseconds from the core, that may appear strongly bent. Beyond this region the jet loses collimation and transitions to a diffuse, low surface brightness morphology.
2. The superluminally moving shocks or "components" present in other blazars are not apparent in the parsec-scale jets of these sources. The components in TeV blazar jets are predominantly stationary or subluminal.
3. The VLBI cores of the three sources studied here are partially resolved and have brightness temperatures of a few times 10^{10} K (compared with a few times 10^{11} K in the case of Mrk 421 and Mrk 501). A high Doppler factor is not required to reduce the observed brightness temperatures below the equipartition value.
4. Counterjets are not observed, and the lower limit placed on the jet to counterjet brightness ratio is $J > \sim 100$.

On the basis of these four points, we conclude that the jets of TeV blazars are only mildly relativistic ($\Gamma \sim 2$–4) on parsec-scales. We suggest the following scenario for the evolution of TeV blazar jets. The jets start out highly relativistic, as required by models reproducing the multiwavelength spectra and variability. Internal or external shocks transfer bulk kinetic energy from the jet with a high efficiency, such that the jet becomes only mildly relativistic a few parsecs from the core. The bulk Lorentz factor has decreased substantially and the shocks have dissipated by the time the jet reaches the parsec scales that we are observing with VLBI, including the VLBI core out to a few milliarcseconds from the core. Immediately beyond this inner jet region, the jet undergoes rapid decollimation, probably because of the low-momentum jet is now interacting with the external environment. This decollimation is evident on the VLBA images of all of these sources beyond a few milliarcseconds from the core. The challenge is now to see if shock-in-jet models can produce deceleration on the scales observed here while also reproducing the other observed multiwavelength properties of these sources, and to explain why the TeV blazars apparently decelerate their jets more efficiently than do the EGRET blazars.

We are currently analyzing additional VLBA data on the TeV blazars, including dual–circular-polarization observations of Mrk 421 after its 2001 TeV high state and observations to further clarify the jet structures in 1ES 1959+650 and PKS 2155−304, as well as in the recently detected TeV blazar H1426+428.

Part of the work described in this paper has been carried out at the Jet Propulsion Laboratory, California Institute of Technology, under contract with the National Aeronautics and Space Administration. The National Radio Astronomy Observatory is a facility of the National Science Foundation operated under cooperative agreement by Associated Universities, Inc. This research has made use of the NASA/IPAC Extragalactic Database (NED), which is operated by the Jet Propulsion Laboratory, California Institute of Technology, under contract with the National Aeronautics and Space Administration. B. G. P. acknowledges support from the NASA Summer Faculty Fellowship Program.

REFERENCES

Aharonian, F. A. et al. 2000, A&A, 353, 847
———. 2003a, A&A, 403, L1
———. 2003b, A&A, 406, L9
Beckmann, V., Wolter, A., Celotti, A., Costamante, L., Ghisellini, G., Maccacaro, T., & Tagliaferri, G. 2002, A&A, 383, 410
Bennett, C. L., et al. 2003, ApJS, 148, 1
Bondi, M., Marcha, M. J. M., Dallacasa, D., & Stanghellini, C. 2001, MNRAS, 325, 1109
Catanese, M., et al. 1998, ApJ, 501, 616
Chadwick, P. M., et al. 1999, ApJ, 513, 161
Chiappetti, L., et al. 1999, ApJ, 521, 552
Dermer, C. D., & Chiang, J. 1998, NewA, 3, 157
Djannati-Ataï et al. 2003a, in ASP Conf. Ser. 290, Active Galactic Nuclei: From Central Engine to Host Galaxy, ed. S. Collin, F. Combes, & I. Shlosman (San Francisco: ASP), 291
———. 2003b, preprint (astro-ph/0307452)
Edelson, R., Griffiths, G., Markowitz, A., Sembay, S., Turner, M. J. L., & Warwick, R. 2001, ApJ, 554, 274
Edwards, P. G., & Piner, B. G. 2002, ApJ, 579, L67
Gaidos, J. A., et al. 1996, Nature, 383, 319
Georganopoulos, M., & Kazanas, D. 2003, ApJ, 594, L27
Ghisellini, G. 2003, preprint (astro-ph/0306429)
Giebels, B., et al. 2002, ApJ, 571, 763
Giommi, P., Padovani, P., & Perlman, E. 2000, MNRAS, 317, 743
Giroletti, M., et al. 2003, ApJ, submitted
Holder, J., et al. 2003a, ApJ, 583, L9
———. 2003b, preprint (astro-ph/0305577)
Horan, D., et al. 2002, ApJ, 571, 753
———. 2003, preprint (astro-ph/0305578)
Itoh, C., et al. 2002, A&A, 396, L1
Jorstad, S. G., Marscher, A. P., Mattox, J. R., Aller, M. F., Aller, H. D., Wehrle, A. E., & Bloom, S. D. 2001b, ApJ, 556, 738
Jorstad, S. G., Marscher, A. P., Mattox, J. R., Wehrle, A. E., Bloom, S. D., & Yurchenko, A. V. 2001a, ApJS, 134, 181
Kataoka, J., Takahashi, T., Makino, F., Inoue, S., Madejski, G. M., Tashiro, M., Urry, C. M., & Kubo, H. 2000, ApJ, 528, 243
Kellermann, K. I., & Pauliny-Toth, I. I. K. 1969, ApJ, 155, L71
Kellermann, K. I., Vermeulen, R. C., Zensus, J. A., & Cohen, M. C. 2000, in Astrophysical Phenomena Revealed by Space VLBI, ed. H. Hirabayashi, P. G. Edwards, & D. W. Murphy (Sagamihara: ISAS), 159
Laurent-Muehleisen, S. A., Kollgaard, R. I., Moellenbrock, G. A., & Feigelson, E. D. 1993, AJ, 106, 875
Lister, M. L. 1998, Ph.D. thesis, Boston Univ.
Lovell, J. E. J. 2000, in Astrophysical Phenomena Revealed by Space VLBI, ed. H. Hirabayashi, P. G. Edwards, & D. W. Murphy (Sagamihara: ISAS), 301
Nishiyama, T., et al. 2000, in AIP Conf. Proc. 516, Proc. 26th International Cosmic-Ray Conference (Salt Lake City), ed. B. L. Dingus, D. B. Kieda, & M. H. Salamon (Melville: AIP), 370
Perlmutter, S., et al. 1997, ApJ, 483, 565
Piner, B. G., Edwards, P. G., Fodor, S., & Rector, T. A. 2002, Publ. Astron. Soc. Australia, 19, 114
Piner, B. G., Unwin, S. C., Wehrle, A. E., Edwards, P. G., Fey, A. L., & Kingham, K. A. 1999, ApJ, 525, 176
Readhead, A. C. S. 1994, ApJ, 426, 51
Rector, T. A., Gabuzda, D. C., & Stocke, J. T. 2003, AJ, 125, 1060
Shepherd, M. C., Pearson, T. J., & Taylor, G. B. 1994, BAAS, 26, 987
Sikora, M., & Madejski, G. 2000, ApJ, 534, 109
Spada, M., Ghisellini, G., Lazzati, D., & Celotti, A. 2001, MNRAS, 325, 1559
Tanihata, C., Takahashi, T., Kataoka, J., & Madejski, G. M. 2003, ApJ, 584, 153
Tanihata, C., Urry, C. M., Takahashi, T., Kataoka, J., Wagner, S. J., Madejski, G. M., Tashiro, M., & Kouda, M. 2001, ApJ, 563, 569
Tingay, S. J., et al. 2001, ApJ, 549, L55
Tommasi, L., Diaz, R., Palazzi, E., Pian, E., Poretti, E., Scaltriti, F., & Treves, A. 2001, ApJS, 132, 73
Tluczykont, M., et al. 2003, preprint (astro-ph/0307334)
Vermeulen, R. C. 1995, Proc. Natl. Acad. Sci., 92, 11385
Villata, M., Raiteri, C. M., Popescu, M. D., Sobrito, G., De Francesco, G., Lanteri, L., & Ostorero, L. 2000, A&AS, 144, 481
Xie, G. Z., Zhou, S. B., Dai, B. Z., Liang, E. W., Li, K. H., Bai, J. M., Xing, S. Y., & Li, W. W. 2002, MNRAS, 329, 689
Xu, C., Baum, S. A., O'Dea, C., Wrobel, J. M., & Condon, J. J. 2000, AJ, 120, 2950
Zhang, Y. H., et al. 2002, ApJ, 572, 762

Note added in proof.——A confirming detection of 1ES 2344+514 at TeV gamma-ray energies was made while this paper was in press (Tluczykont et al. 2003)